Spin dynamics in the multiferroic materials (invited)

Feng Ye, Randy S. Fishman, Jason Haraldsen, Bernd Lorenz, C. W. Chu et al.

Citation: J. Appl. Phys. **111**, 07E137 (2012); doi: 10.1063/1.3677863
View online: http://dx.doi.org/10.1063/1.3677863
View Table of Contents: http://jap.aip.org/resource/1/JAPIAU/v111/i7
Published by the American Institute of Physics.

Spin dynamics in the multiferroic materials (invited)

Feng Ye,[1,a)] Randy S. Fishman,[2] Jason Haraldsen,[2] Bernd Lorenz,[3] C. W. Chu,[3] and Tsuyoshi Kimura[4]
[1]*Neutron Scattering Science Division, Oak Ridge National Laboratory, Oak Ridge, Tennessee 37831, USA*
[2]*Materials Science and Technology Division, Oak Ridge National Laboratory, Oak Ridge, Tennessee 37831, USA*
[3]*Department of Physics and TCSUH, University of Houston, Houston, Texas 77204, USA*
[4]*Division of Materials Physics, Graduate School of Engineering Science, Osaka University, Osaka 560-8531, Japan*

(Presented 3 November 2011; received 26 September 2011; accepted 21 November 2011; published online 8 March 2012)

We report high resolution inelastic neutron scattering measurements and spin dynamics calculations in two multiferroic materials: the geometrically frustrated triangular lattice $CuFeO_2$ and mineral Hübnerite $MnWO_4$. In un-doped $CuFeO_2$ a low-T collinear spin structure is stabilized by long range magnetic interactions. When doped with a few percent of gallium, the spin order evolves into a complex noncollinear configuration and the system becomes multiferroic. Similarly, the ground state collinear spin order in pure $MnWO_4$ results from delicate balance between competing magnetic interactions up to 11th nearest neighbors and can be tuned by substitution of Mn ions with magnetic or nonmagnetic impurities. The comprehensive investigation of spin dynamics in both systems help to understand the fundamental physical process and the interactions leading to the close interplay of magnetism and ferroelectricity in this type of materials. © *2012 American Institute of Physics*. [doi:10.1063/1.3677863]

I. INTRODUCTION

Magnetoelectric multiferroic materials, which exhibit the coexistence of ferroelectric (FE) and magnetic orders, have attracted great attention in recent years.[1–4] Several classes of multiferroics among transition metal oxides have been discovered including geometrically frustrated $CuMO_2$ (M: Fe, Cr),[5,6] $Ni_3V_2O_8$,[7] or rare-earth (R) manganites $RMnO_3$ and RMn_2O_5.[8–10] The ability to simultaneously control the electric (E) and magnetic (M) properties makes these multiferroics promising candidates for technological applications.[8,11] A characteristic feature in those magnetically induced multiferroics is the presence of long-range magnetic structures with noncollinear spiral spin configurations. Such magnetic order is a consequence of magnetic frustration resulting in a close competition of different magnetic structures that are nearly degenerate in energy.

Both mineral delaffosite $CuFeO_2$ and Hübnerite $MnWO_4$ belong to the frustrated spin system. The frustration in the former stems from geometric constraint while it is attributed to the competing magnetic interactions in the latter case. In $CuFeO_2$, antiferromagnetically (AFM) coupled Fe^{3+} ions form a triangular lattice in the ab-plane [Fig. 1(a)]. The system enters an Ising like 4-sublattice ($\uparrow\uparrow\downarrow\downarrow$) order below 11 K with magnetic propagation wavevector $q_M = (1/4, 1/4, 3/2)$.[12] Such spin order is different from other triangular lattice antiferromagnet (TLA) where three neighboring spins align at 120° from each other in the basal plane.[13] With application of a magnetic field greater than 7 T along c axis, the spin structure changes to a complex noncollinear (CNC) configuration with magnetic wavevector appearing at $q_{m1} = (0.2, 0.2, 1.5)$ and $q_{m2} = (0.3, 0.3, 1.5)$, where spin rotation axis is along the [1,1,0] direction.[14] The magnetic field induced electric polarization P has the same direction of spin rotation axis and cannot be explained by prevailing microscopic spin current model or the inverse Dzyaloshinskii-Moriya interaction,[15–17] which states that P is perpendicular to both the chiral axis $S_i \times S_j$ and the magnetic order wavevector Q. It was proposed that the spin-driven multiferroic behavior arises from the uniform charge transfer through the metal-ligand hybridization in the presence of spin-orbit coupling.[18] Similar to the magnetic field, doping with a few percent of nonmagnetic Al^{3+} or Ga^{3+} at the Fe^{3+} site can drive the system into electric polar state.[19–21] Exotic magnetoelectric control has recently been reported in the Ga-doped $CuFeO_2$ to achieve magnetic digital flop of ferroelectric domains.[22] On the other hand, the Hübnerite $MnWO_4$ also appears to be an interesting system that exhibits multiferroic phenomena and shows rich magnetic phases via chemical substitutions or magnetic field.[23–29] It is regarded as one of the prototypical multiferroics capable of magnetoelectric (ME) control.[29,30] The Mn^{2+} spins in pure $MnWO_4$ undergo successive transitions in zero field.[34] The low-T magnetic structure has collinear configuration and evolves into an incommensurate (ICM) spiral order accompanied by a spontaneous electric polarization P along the b-axis for $7.8\,K < T < 12\,K$. When T is further raised between 12 K and 13.5 K, $MnWO_4$ orders in a collinear ICM state and is paraelectric. The electric polarization that is correlated with the spiral structure can be well understood by the inverse DM mechanism.

Despite the extensive investigations of the bulk properties, characterizing the magnetic interactions that is essential to

a)Author to whom correspondence should be addressed. Electronic mail: yef1@ornl.gov.

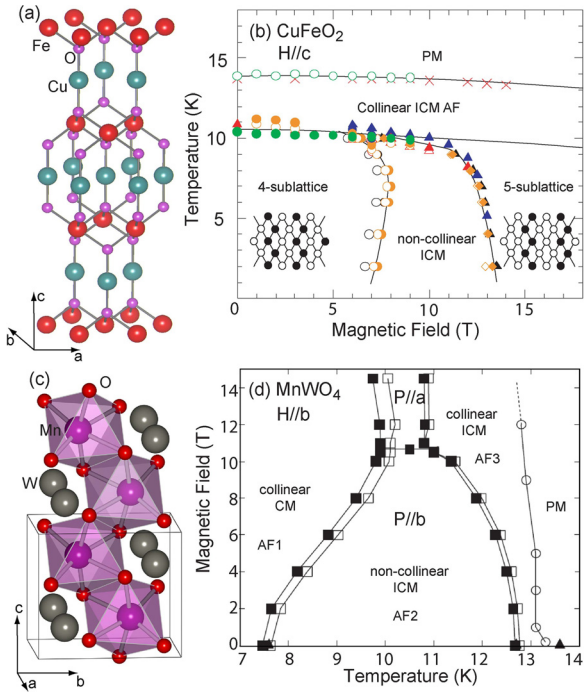

FIG. 1. (Color online) (a) The crystal structure of $CuFeO_2$. (b) Temperature (T) vs magnetic field (B) phase diagram of $CuFeO_2$ with B applied along the c axis [from Ref. 5]. (c) The crystal structure of $MnWO_4$. (b) T vs B phase diagram of $MnWO_4$ with B applied along the b axis [from Ref. 23].

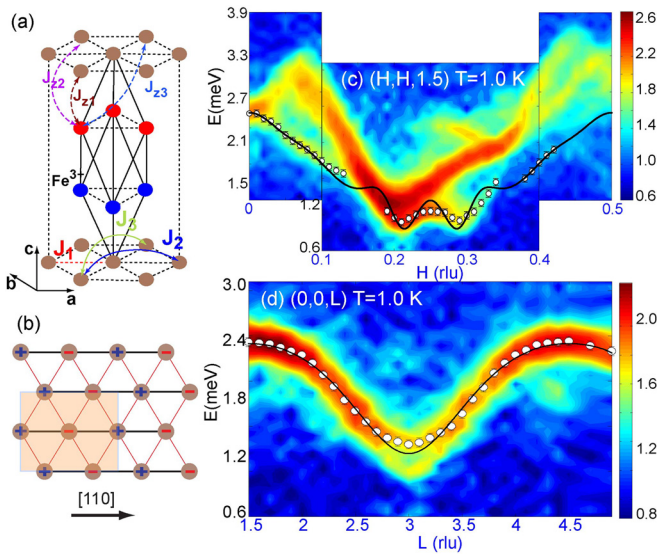

FIG. 2. (Color online) (a) Schematics of the crystal structure (only Fe ions shown for clarity) and the relevant magnetic exchange interactions between neighboring Fe ions. (b) The ↑↑↓↓ spin configuration (with moment pointing along c-axis) within the hexagonal plane. The magnetic unit cell in shown in shaded area. (c) Spin-wave dispersion (SW) along the [1, 1, 0] direction. (d) SW dispersion along the [0, 0, 1] direction. Points are experimental data and the solid lines denotes a fit to the model described in the text.

understand the various magnetic phase transitions remains an unresolved issue. In this article, we summarize our inelastic neutron scattering (INS) studies in order to unravel the microscopic origin for the low-T spin structure and effect of chemical doping in those multiferroic materials. Most importantly, such microscopic characterization of the magnetic dynamics provides a fundamental step toward the construction of the ground state Hamiltonian from which the FE phase can be derived.

Single crystals of $CuFe_{1-x}Ga_xO_2$ ($x = 0$, 0.035, from Osaka University) and $Mn_{1-x}Fe_xWO_4$ ($x = 0$, 0.035, 0.05, 0.10, from University of Houston) were grown by floating zone technique. The INS measurements were performed at the Cold Neutron Chopper Spectrometer (CNCS) at the Oak Ridge National Laboratory[31] and the Disk Chopper Spectrometer (DCS) at the NIST Center for Neutron Research.[32] We aligned the crystals in different scattering planes such that the spin-wave (SW) dispersion along several symmetry directions that pass across the magnetic Bragg peaks can be measured. The incident neutrons with wavelength of $\lambda = 4.4$ Å was chosen to ensure the needed energy resolution to separate various magnetic excitation branches. The data obtained from CNCS and DCS are reduced and analyzed using the DAVE software package.[33]

We start spin dynamics investigation in pure $CuFeO_2$ which forms ↑↑↓↓ phase at low-T. The contour plot in Figs. 2(c)–2(d) show the measured SW spectra within and perpendicular to the hexagonal plane, respectively.[35,36] The highly dispersive excitation in the [0, 0, 1] direction indicates a substantial inter-layer coupling. Surprisingly, the in-plane SW dispersion along the [1, 1, 0] direction exhibits two energy minima with a finite energy gap of 0.9 meV at symmetric wavevector transfer $q_{m1} = (0.2, 0.2, 1.5)$ and $q_{m2} = (0.3, 0.3, 1.5)$ around the magnetic Bragg peak. Recall q_{m1} and q_{m2} are precisely the same wavevectors associated with the ICM magnetic order in the CNC phase. Such a feature in the excitation spectra could be interpreted as a dynamical precursor to the magnetoelectric behavior.

When doped with small amount of nonmagnetic Ga, the spin structure is considerably modified and evolves into CNC phase shown in Figs. 3(a)–3(b). Such change is related to the lattice distortion that is directly associated with the displacements of the oxygen atoms.[37,38] Viewing along the [1, 1, 0] direction, the turning angles of spin fluctuate about $\Delta\theta_1 = 22°$ and $\Delta\theta_2 = 134°$ that is due to the modulation created by the spin harmonics. The spin configuration of CNC phase can be modeled using

$$S_z(\mathbf{R}) = A\{\cos(Q\cdot x) + \sum_{l=1} C_{2l+1}\cos[Q(2l+1)\cdot x] - \sum_{l=0} B_{2l+1}\sin[(2\pi - Q)(2l+1)\cdot x]\}. \quad (1)$$

Here, the C_{2l+1} harmonics are produced by the anisotropy energy D and the B_{2l+1} harmonics are produced by the lattice distortion K_1.[14] The square of these harmonics are proportional to the observed elastic intensities at odd multiples of $q_{m1} = (0.2, 0.2, 1.5)$ and $q_{m2} = (0.3, 0.3, 1.5)$]. A is normalized such that the maximum of $|S_z(\mathbf{R})|$ is S = 5/2. The perpendicular spin S_y is given by

$$S_y(\mathbf{R}) = \sqrt{S - S_z(\mathbf{R})^2}\,\mathrm{sgn}(g(\mathbf{R})), \quad (2)$$

where

$$g(\mathbf{R}) = \sin(Q\cdot x) + G_1\cos[(2\pi - Q)\cdot x], \quad (3)$$

and G_1 is an additional variational parameter.

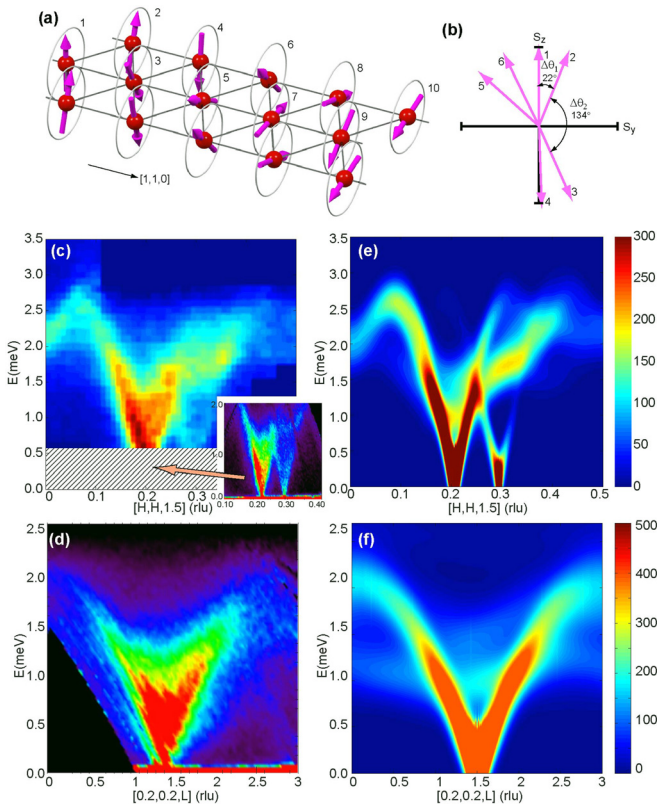

FIG. 3. (Color online) (a) CNC spin configurations in the 3.5%-Ga doped $CuFeO_2$ within the hexagonal plane. (c) SW dispersion along the [H, H, 1.5] direction. Inset shows the high resolution data using cold neutron inelastic scattering near $q_1 = [0.2, 0.2, 1.5]$ and $q_2 = [0.3, 0.3, 1.5]$. (d) SW dispersion along [0.2, 0.2, L] direction. (e)-(f) display the predicted excitation spectra using intra-layer and inter-layer interaction along with a lattice distortion and anisotropy (see text).

Figures 3(c)–3(d) display the magnetic excitation spectra measured in $CuFe_{0.965}Ga_{0.035}O_2$. It is evident that two energy dips observed at q_{m1} and q_{m2} in the parent compound now collapse to the elastic position ($E = 0$). There is also a "shoulder" at $H \approx 0.08$ and an intensity "hole" around "$H \approx 0.30$" and $E = 1.0$ meV.

To characterize the SWs in the collinear and CNC phases, we use the general effective Heisenberg Hamiltonian

$$H = -1/2 \sum_{i,j} J_{i,j} \vec{S}_i \cdot \vec{S}_j - D \sum_i S_{iz}^2, \qquad (4)$$

where $\Sigma_{i,j}$ indicates summation over pairs of spins, D is the single-ion anisotropy, and S_{iz} denote the spin components along the easy axis. The corresponding spectral weight is obtained using spin rotation technique[39] and can be expressed as

$$\frac{d^2\sigma}{d\Omega dE} \propto f^2(Q) e^{-2W} \sum_{\alpha\beta} (\delta_{\alpha\beta} - \hat{Q}_\alpha \hat{Q}_\beta) S^{\alpha\beta}(\mathbf{Q}, \omega), \qquad (5)$$

where $f^2(Q)$ is the form factor for the magnetic ions, e^{-2W} is the Debye-Waller factor, $\hat{Q}_\alpha$ is the α component of a unit vector in the direction of $\mathbf{Q}$, $S^{\alpha\beta}(\mathbf{Q}, \omega)$ is the response function that describes the $\alpha\beta$ spin-spin correlations.

Table I compares the Hamiltonian parameters obtained for the parent and the doped $CuFeO_2$. Except much reduced anisotropy term D, the in-plane magnetic exchange coupling in 3.5%-Ga doped sample are similar to the un-doped one. The comparable inter-plane J_{z1} also underscores the three dimensional character of this system. It is notable that J_{z2} and J_{z3} are somewhat weakened, which can be attributed to the disorder caused by Ga doping. Figures 3(e)–3(f) show the calculated spectra map using Eq. (5) with fitted parameters. The remarkable agreement between observation and prediction indicates that INS studies provide a distinct dynamical fingerprint of the CNC multiferroic phase.

TABLE I. Comparison of Hamiltonian parameters (in units of meV) of pure $CuFeO_2$ and doped $CuFe_{1-x}Ga_xO_2$.

x	J_1	J_2	J_3	J_{z1}	J_{z2}	J_{z3}	D
0	−0.23	−0.12	−0.16	−0.06	0.07	−0.05	0.22
0.035	−0.19	−0.10	−0.13	−0.13	0.02	−0.01	−0.01

We next examine the spin dynamics in the pure and Fe-doped $MnWO_4$.[40] The ground state spin configuration of undoped system is collinear and CM with two inequivalent commensurate (CM) wavevectors $q_M = (1/4, 1/2, \pm 1/2)$ [Fig. 4(a)]. With substitution of Fe ions, the CM phase expands in the x-T phase diagram while the spiral phase at intermediate temperature is suppressed. Figures 5(a)–5(b) display the spin excitation spectra along the [1, K, 2] and [H,1, −2 H] directions with $K = 0.5$ and $H = 0.25$. Both scans

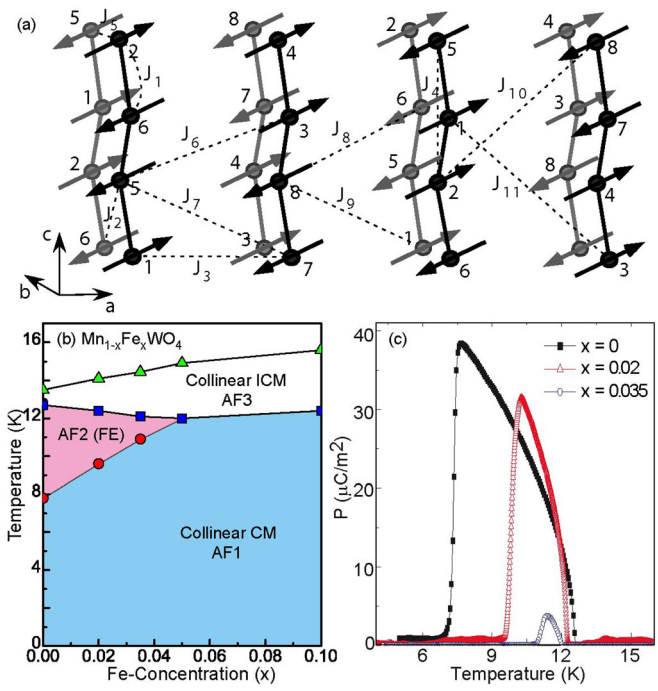

FIG. 4. (Color online) (a) The magnetic structure of pure $MnWO_4$ in the collinear CM phase. The Mn^{2+} spins lie in the ac plane with moments canted to the a axis about 35° (Ref. 34) The spins form zigzag ↑↑↓↓ chains along the c axis and are coupled antiferromagnetically along the b axis. The magnetic interactions along and between spin chains are labeled with increasing Mn-Mn distance. (c) The T-x phase diagram of iron-doped $Mn_{1-x}Fe_xWO_4$. (d) Temperature dependence of electric polarization (P) in the Fe-doped $MnWO_4$. Notice the quick suppression of P with increasing Fe-concentration (Ref. 42).

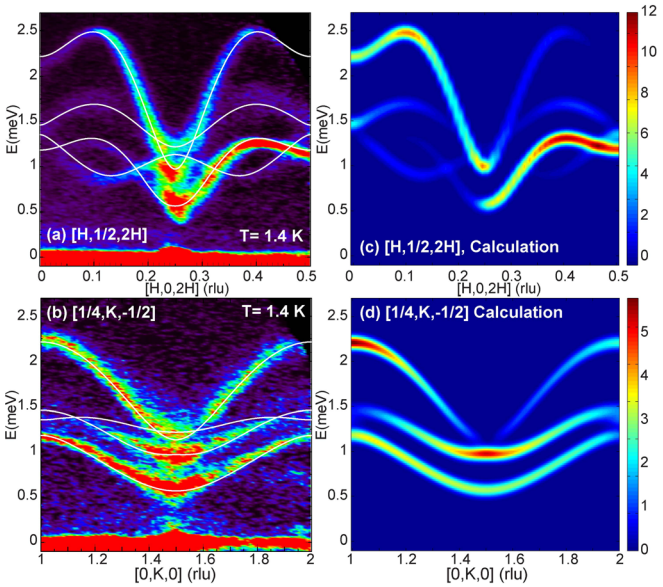

FIG. 5. (Color online) (a) SW dispersion spectra along the $[1,0,2]$ direction through the magnetic peak $(1/4, 1/2, 1/2)$. (b) Magnetic excitation spectra along the $[0,1,0]$ direction through the magnetic Bragg reflection $(1/4, 1/2, -1/2)$. (c)-(d) Calculated spectra along the same symmetry directions as in (a) and (b).

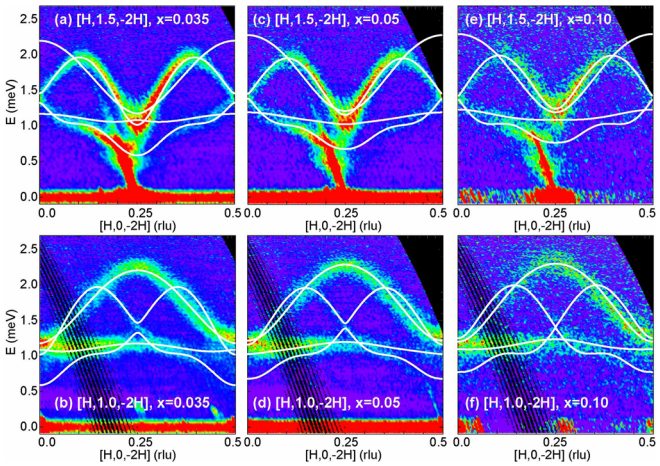

FIG. 6. (Color online) Evolution of magnetic excitation spectra in $Mn_{1-x}Fe_xWO_4$ for $x = 0.035$, 0.05, 0.10. (a)-(b) SW dispersion spectra along $[1, K, -2]$ with $K = 1.5$ and 1.0 for $x = 0.035$. (c)-(d) Similar dispersion spectra for $x = 0.05$, (e)-(f) are spectra for $x = 0.10$. Solid (white) lines are calculated SW dispersions.

go through the magnetic Bragg peaks. The data show four distinct branches that disperse out from the magnetic zone center (ZC) to the zone boundary (ZB). The spectra reveal a spin gap of 0.5 meV and boundary energy around 2.2 meV. The excitation bandwidth is consistent with the energy scale for the ordering temperature of 13.5 K. The intensity of the excitation spectra is highly asymmetric with respect to the magnetic Bragg point. For example, the spectral weight of lowest branch in Fig. 5(a) is missing as H approaches zero while it shows the highest intensity as it moves toward $H = 0.5$. This highlights the importance of a complete survey in reciprocal space to fully map out the magnetic dynamics. The intensity map in Fig. 5(b) shows similar asymmetric feature on both sides of the magnetic ZC.

Combining data along all symmetry directions, the SW dispersion relations can be simultaneously modeled using Eq. (4). Analysis using nine exchange parameters and single-ion anisotropy D as assumed in previous work [Ref. 41] does not capture the dispersion relations in all directions. Hence, an extra pair of magnetic interactions J_{10} and J_{11} is included in order to achieve satisfactory agreement with the measured data. As shown in Table II, the magnetic exchange constants generally decrease in amplitude as the bonding distance increases, except the weaker J_2 and J_5 along the b-axis. Since the electronic configuration of Mn^{2+} ion is $3d^5$ (orbital singlet), one should not expect it to have any magnetic anisotropy. The non-vanishing $D = 0.09$ meV indicates a possible spin-orbit coupling that causes the pinning of the magnetic moments in the ac-plane.[43] To test whether the refined exchange parameters indeed correspond to the ground state CM spin structure, we calculate the magnetic energy for all possible spin configurations (total of $2^8 = 256$ with eight spins in one magnetic unit cell). Only the spin structure depicted in Fig. 4(a) gives the lowest energy verifying we have obtained correct parameters. Figures 5(c)–5(d) show the calculated excitation spectra map using Eq. (5). The excellent agreement between the calculation and the experimental data provides convincing evidence that the collinear spin structure is stabilized by the delicate balance between competing interactions up to 11th nearest neighbor.

To better understand the bulk property where P is suppressed with increasing Fe-doping, it is instructive to investigate how the introduction of Fe ions affects the magnetic interactions. Systematic studies of the spin dynamics for the doped $Mn_{1-x}Fe_xWO_4$ are performed with x ranging from 0.035 to 0.10. Figures 6 and 7 illustrate the evolution of excitations along the [1,0,−2] and [0,1,0] directions. With increasing x, the well defined spectra present in the parent compound weaken in intensity and broaden in peak width. In addition, the energy gap at the ZC increases from $E = 0.57$ meV for $x = 0$ to $E = 0.77$ meV for $x = 0.10$ while the ZB energy increases accordingly. Nevertheless, the modification of the spin dynamics is rather subtle and can only be appreciated by high resolution measurements. Some

TABLE II. The doping dependence of magnetic exchange coupling parameters in $Mn_{1-x}Fe_xWO_4$ derived from spin wave model calculation according to Eq. (1). The Mn^{2+} ions located at position (1/2, 0.685, 1/4) interact with neighboring spins through one or two oxygens. The bonding distance (in units of Å) between Mn…Mn are also listed.

	J_1	J_2	J_3	J_4	J_5	J_6	J_7	J_8	J_9	J_{10}	J_{11}	D	χ^2
Mn…Mn	3.286	4.398	4.830	4.990	5.760	5.801	5.883	6.496	6.569	6.875	7.013		
$x = 0$	−0.42	−0.04	−0.32	−0.26	0.05	−0.43	−0.12	0.02	−0.26	−0.15	0.02	0.09	1.11
$x = 0.035$	−0.43	−0.04	−0.32	−0.24	0.06	−0.42	−0.12	0.02	−0.27	−0.13	0.02	0.11	1.31
$x = 0.05$	−0.41	−0.04	−0.32	−0.21	0.06	−0.40	−0.11	0.02	−0.28	−0.12	0.04	0.13	1.35
$x = 0.10$	−0.37	−0.03	−0.31	−0.20	0.07	−0.35	−0.10	0.02	−0.30	−0.11	0.05	0.16	1.43

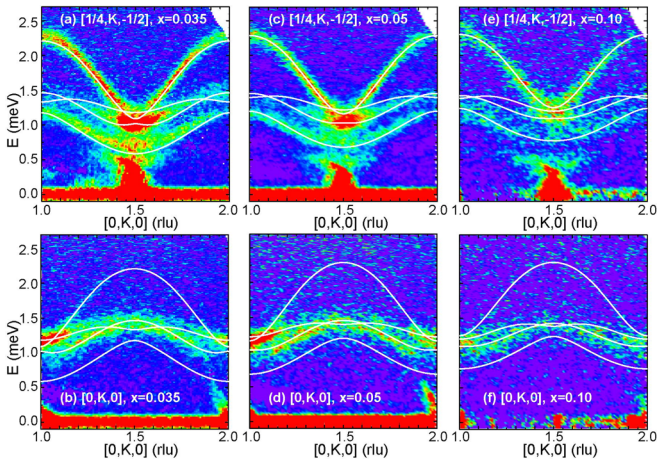

FIG. 7. (Color online) Evolution of magnetic excitation spectra along [H,1,−2 H] directions in $Mn_{1-x}Fe_xWO_4$ for $x = 0.035$, 0.05, 0.10. (a)-(b) SW dispersion spectra with $H = 0.25$ and 0.0 for $x = 0.035$. (c)-(d) Similar dispersion spectra for $x = 0.05$, (e)-(f) are spectra for $x = 0.10$. Solid (white) lines are calculated SW dispersions.

characteristic Hamiltonian parameters are plotted in Fig. 8 to better see the doping effect. One notices that single ion anisotropy D increases nearly monotonically with increasing x, suggesting that the magnetic moments are likely to be pinned along the easy axis. Such a trend is consistent with the collinear spin structure found in the Fe-rich compounds. In addition, the strength of all dominant AFM interactions decreases at higher concentration. The ratio of magnetic interactions J_4/J_1 (the second and first NN interactions in c axis) becomes smaller. This observation reveals that the system becomes less frustrated along the ↑↑↓↓ chain, and the collinear spin order is more preferable at higher Fe concentration.

A complex spin configuration would form in the 1 D frustrated spin chain if the next-nearest-neighbor (NNN) AFM interaction J' becomes substantially stronger compared to the nearest-neighbor (NN) ferromagnetic (FM) exchange coupling J. A spiral phase might appear for $J'/|J| > 1/4$ and a collinear ↑↑↓↓ structure will emerge when $J'/|J| > 1/2$.[3] The zigzag E-type phase observed in rare earth manganite $RMnO_3$ is a classic example of competing short-range FM/AFM interactions caused by lattice distortions.[44,45] In the case the $MnWO_4$, the exchange coupling are predominantly AFM and three dimensional (Table II). Nevertheless, strong long-range magnetic interactions comparable to NN interaction (J_1) along the c-axis ($|J_4| > 1/2$) and a-axis are observed. This reflects the magnetic frustration in those two directions and is consistent with the ICM components in a and c but not in the b direction, when the system enters the spiral phase. The exchange coupling remains sizable (J_{10}) even at a rather long distance. Such an unusual extended interaction could also be viewed as a much reduced NN exchange coupling because of nearly 90° Mn-O-Mn bonding angle.[46] Thus, the unique crystalline structure of $MnWO_4$ makes it possible to achieve novel physical properties with modified magnetic interactions. For instance, the introduction of nonmagnetic Zn^{2+} ions that weaken the overall magnetic interactions switches the ground state from collinear to spiral order.,[26,27] while replacing Mn^{2+} with Fe^{2+} ions that have a larger local magnetic anisotropy enhance the collinear structure, as found in our INS work.

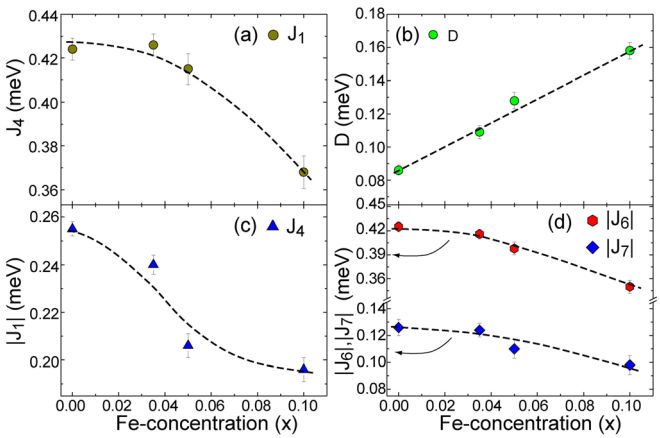

FIG. 8. (Color online) Doping dependence of the characteristic magnetic exchange parameters (see Fig. 4(a) for detailed exchange path). (a) The nearest neighbor (NN) interaction J_1. (b) Single ion anisotropy D. (c) the 4th NN exchange coupling constant J_4, which marks the second competing magnetic interaction along the zigzag chain along c axis. (d) The amplitude of 6th and 7th NN exchange coupling $|J_6|$ and $|J_7|$, those are next competing magnetic interactions between zigzag chains along a axis. Dash lines are guides to the eyes.

In summary, high resolution INS is used to study the SWs in the multiferroic $CuFe_{1-x}Ga_xO_2$ and $Mn_{1-x}Fe_xWO_4$. An effective Hamiltonian is employed to describe the SW dispersion relations. We identified the magnetic interactions that are responsible for the low-T spin structures. The collinear spin order observed in both systems is stabilized by the delicate balance of competing long-range magnetic interactions and subject to perturbations. The complex ground state observed in the Ga-doped $CuFeO_2$ provides an alternative way to realize multiferroic coupling, where the displacements of the oxygen atoms distort the spin configuration and produce the electric polarization. Consequently, spin system with similar rhombohedral or hexagonal symmetries may also exhibit the same form of multiferroic coupling. In the case of $MnWO_4$, our results indicate that chemical substitution is a viable tool to tune the multiferroic properties in this extremely sensitive system. Rich and complex magnetic phases are expected in the doped samples resulting from the fine tuning of the exchange coupling.

This work was sponsored by the U.S. Department of Energy, Office of Basic Energy Sciences, Materials Sciences and Engineering Division and Scientific User Facilities Division. Work at Houston was supported in part by the T.L.L. Temple Foundation, the J.J. and R. Moores Endowment, and the State of Texas through TCSUH and at LBNL through the US DOE, Contract No. DE-AC03-76SF00098. We acknowledge the support of the National Institute of Standards and Technology, U.S. Department of Commerce, in providing the neutron research facilities used in this work.

[1]Y. Tokura, Science **312**, 1481 (2006).
[2]D. I. Khomskii, J. Magn. Magn. Mater. **306**, 1 (2006).
[3]S.-W. Cheong and M. Mostovoy, Nature Materials **6**, 13 (2007).
[4]T. Kimura, Annu. Rev. Mater. Res. **37**, 387 (2007).

[5]T. Kimura, J. C. Lashley, and A. P. Ramirez, Phys. Rev. B **73**, 220401(R) (2006).
[6]K. Kimura, H. Nakamura, K. Ohgushi, and T. Kimura, Phys. Rev. B **78**, 140401(R) (2008).
[7]G. Lawes *et al*., Phys. Rev. Lett. **95**, 087205 (2005).
[8]Kimura *et al*., Nature (London) **426**, 55 (2003).
[9]T. Goto, T. Kimura, G. Lawes, A. P. Ramirez, and Y. Tokura, Phys. Rev. Lett. **92**, 257201 (2004).
[10]N. Hur *et al*., Nature (London) **429**, 392 (2004).
[11]Y. Yamasaki *et al*., Phys. Rev. Lett. **98**, 147204 (2007).
[12]S. Mitsuda, H. Yoshizawa, N. Yaguchi, and M. Mekata, J. Phys. Soc. Jpn. **60**, 1885 (1991).
[13]M. F. Collins and O. A. Petrenko, Can. J. Phys. **75**, 605 (1997); H. Kawamura, J. Phys.: Condens. Matter **10**, 4707 (1998).
[14]J. T. Haraldsen *et al*., Phys. Rev. B **82**, 020404(R) (2010); J. T. Haldsen *et al*, *ibid*. **82**, 144441 (2010).
[15]H. Katsura, N. Nagaosa, and A. V. Balatsky, Phys. Rev. Lett. **95**, 057205 (2005).
[16]I. A. Sergienko and E. Dagotto, Phys. Rev. B **73**, 094434 (2006).
[17]M. Mostovoy, Phys. Rev. Lett. **96**, 067601 (2006).
[18]T. Arima, J. Phys. Soc. Jpn. **76**, 073702 (2007).
[19]N. Terada *et al*., J. Phys. Soc. Jpn. **74**, 2604 (2005).
[20]N. Terada *et al*., Phys. Rev. B **78**, 014101 (2008).
[21]T. Nakajima *et al*., Phys. Rev. B **79**, 214423 (2009).
[22]S. Seki *et al*., Phys. Rev. Lett. **103**, 237601 (2009).
[23]K. Taniguchi *et al*., Phys. Rev. Lett. **97**, 097203 (2006); A. H. Arkenbout *et al*, Phys. Rev. B **74**, 184431 (2006); O. Heyer *et al*, J. Phys.: Condens. Matter **18**, L471 (2006).
[24]F. Ye *et al*., Phys. Rev. B **78**, 193101 (2008).
[25]Y.-S. Song, J.-H. Chung, J. M. S. Park, and Y.-N. Choi, Phys. Rev. B **79**, 224415 (2009).
[26]L. Meddar *et al*., Chem. Mater. **21**, 5203 (2009).
[27]R. P. Chaudhury *et al*., Phys. Rev. B **83**, 014401 (2011).
[28]T. Finger *et al*., Phys. Rev. B **81**, 054430 (2010).
[29]H. Sagayama *et al*., Phys. Rev. B **77**, 220407(R) (2008).
[30]K. Taniguchi, N. Abe, H. Umetsu, H. A. Katori, and T. Arima, Phys. Rev. Lett. **101**, 207205 (2008).
[31]G. Ehlers *et al*., Rev. Sci. Instrum. **82**, 085108 (2011).
[32]J. R. D. Copley and J. C. Cook, Chem. Phys. **292**, 477 (2003).
[33]R. T. Azuah *et al*., J. Res. Natl. Inst. Stand. Technol. **114**, 341 (2009).
[34]G. Lautenschläger *et al*., Phys. Rev. B **48**, 6087 (1993).
[35]F. Ye *et al*., Phys. Rev. Lett. **99**, 157201 (2007); R. F. Fishman *et al*, Phys. Rev. B **78**, 140407 (2008).
[36]T. Nakajima *et al*., J. Phys. Soc. Jpn. **80**, 014714 (2011).
[37]F. Ye *et al*., Phys. Rev. B **73**, 220404(R) (2006).
[38]N. Terada *et al*., J. Phys. Soc. Jpn. **75**, 023602 (2006).
[39]J. T. Haraldsen and R. S. Fishman, J. Phys.: Condens. Matter **21**, 216001 (2009).
[40]F. Ye *et al*., Phys. Rev. B **83**, 140401(R) (2011).
[41]H. Ehrenberg, H. Weitzel, H. Fuess, and B. Hennion, J. Phys.: Condens. Matter **11**, 2649 (1999).
[42]R. P. Chaudhury *et al*. New J. Phys. **11**, 033036 (2008).
[43]N. Hollmann *et al*., Phys. Rev. B **82**, 184429 (2010).
[44]T. Kimura *et al*., Phys. Rev. B **68**, 060403(R) (2003).
[45]M. Mochizuki, N. Furukawa, and N. Nagaosa, Phys. Rev. Lett. **105**, 037205 (2010).
[46]J. B. Goodenough, *Magnetism and Chemical Bond* (Interscience, New York, 1963).